Sustainable Cities and Society 1 (2011) 104–115

Contents lists available at ScienceDirect

Sustainable Cities and Society

journal homepage: www.elsevier.com/locate/scs

# Development of a model for urban heat island prediction using neural network techniques

K. Gobakis [a], D. Kolokotsa [b,*], A. Synnefa [c], M. Saliari [c], K. Giannopoulou [c], M. Santamouris [c]

[a] Technical University of Crete, Electronics and Computer Engineering Department, GR 73100, Crete, Greece
[b] Technical University of Crete, Environmental Engineering Department, Renewable and Sustainable Energy Laboratory, GR 73100, Crete, Greece
[c] National and Kapodistrian University of Athens, Greece, Physics Department Section of Applied Physics, Physics Department, Build. Physics 5, 15784, Athens, Greece

ARTICLE INFO

*Keywords:*
Artificial neural networks
Urban heat island phenomenon
Prediction of urban heat island

ABSTRACT

The urban heat island (UHI) phenomenon is mainly caused by the differences in the thermal behaviour between urban and rural settlements that are associated with the thermal properties of urban materials, urban geometry, air pollution, and the anthropogenic heat released by the urban activities. The UHI has a serious impact on the energy consumption of buildings, increases smog production, while contributing to an increasing emission of pollutants from power plants, including sulfur dioxide, carbon monoxide, nitrous oxides and suspended particulates.

This study presents the applicability of artificial neural networks (ANNs) and learning paradigms for UHI intensity prediction in Athens, Greece. The proposed model is tested using Elman, Feed-Forward and Cascade neural network architecture. The data of time, ambient temperature and global solar radiation are used to train and test the different models. The prediction accuracy is analyzed and evaluated.



## 1. Introduction

The urban heat island (UHI) phenomenon serves as a trap for atmospheric pollutants, deteriorates the quality of life and has a socio-economic impact in the urbanised areas (Santamouris, Paraponiaris, & Mihalakakou, 2007; Santamouris, Pavlou, Synnefa, Niachou, & Kolokotsa, 2007). Important research has been accomplished over the last hundred years to quantify its impact on the urban climate (Akbari, Konopacki, & Pomerantz, 1999; Mihalakakou, Flokas, Santamouris, & Helmis, 2000; Santamouris, 2001). Various heat island studies have been performed in Europe during the last 15 years (Santamouris, 2007). Urban heat island and increased urban temperatures (Livada, Santamouris, & Assimakopoulos, 2007; Livada, Santamouris, Niachou, Papanikolaou, & Mihalakakou, 2002; Mihalakakou, Santamouris, & Papanikolaou, 2004), exacerbate the cooling load of buildings, increase the peak electricity demand for cooling and decrease the efficiency of air conditioners (Cartalis, Synodinou, Proedrou, Tsangrassoulis, & Santamouris, 2001; Hassid et al., 2000; Kolokotroni, Giannitsaris, & Watkins, 2006; Santamouris et al., 2001). Moreover the urban agglomeration has a negative impact on the cooling effectiveness of natural and night ventilation (Geros, Santamouris, Karatasou, Tsangrassoulis, & Papanikolaou, 2005) and contributes to the increase of outdoor pollutants' concentration (Crutzen, 2004; Taha, 1994).

Consequently, the prediction of the urban heat island behaviour has gained a significant attention. Although a number of modelling approaches for urban heat island do exist (Mirzaei & Haghighat, 2010), the complexity of the phenomenon, the bulk of urban details required to attain an accurate urban model and the increased cost and computational time of the analytical modelling approaches has led to the exploration of other prediction methods.

Artificial neural networks (ANNs) have been used in a number of prediction studies that involve atmospheric time series data. Yi and Prybutok (1996) predicted daily maximum ozone levels in Texas metropolitan areas with a standard three-layer ANN model with nine inputs and four hidden nodes and found it to be superior to statistical methods. A three-layer ANN model with 17 inputs was developed by Jiang et al. (2004) to predict the air pollution levels of cities in China. Inputs to the models were not site-specific, allowing the model to be applied to a number of locations across China. Air temperature, wind speed, and relative humidity in Saskatchewan, Canada were predicted for 24 h in advance by ANN models developed and applied by Maqsood, Khan, and Abraham (2004). They found that combining the outputs of a standard Feed-Forward ANN, a recurrent ANN, a radial basis function network, and a Hopfield network into a simple "winner-take-all" ensemble led to more accurate predictions of wind speed, relative humidity, and air temperature than any of the individual component networks. Ruano, Crispim, Conceicão, and Lúcio (2006) used a multi-objective genetic

* Corresponding author.
*E-mail address:* dkolokotsa@enveng.tuc.gr (D. Kolokotsa).

2210-6707/$ – see front matter © 2011 Elsevier B.V. All rights reserved.
doi:10.1016/j.scs.2011.05.001

algorithm to develop a radial basis function ANN model for the prediction of air temperature in a secondary school building in Portugal. Air-conditioning control scheme simulations indicated that temperatures could be more consistently managed and that air conditioner run times could be reduced using an ANN model. Tasadduq, Rehman, and Bubshait (2002) used a back propagation ANN with batch learning scheme for 24-h prediction in ambient temperature on a coastal location in Saudi Arabia. They found that temperature can be predicted even with only one input with good accuracy.

Additionally, a number of urban heat island prediction studies are based in the ANN technology (Santamouris, Mihalakakou, & Papanikolaou, 1999). A neural network architecture was developed to predict the urban heat island intensity in Athens, Greece, during both day and night (Mihalakakou et al., 2004) using data for a two-year time period. Another study uses input data from meteorological stations as well as historic measured air temperatures within the city to predict the urban heat island intensity in London based on neural network architecture (Kolokotroni, Davies, Croxford, Bhuiyan, & Mavrogianni, 2010).

It should be underlined here that most urban heat island NN prediction studies require a large set of data to train the neural networks and predict the phenomenon in an accurate and acceptable manner. The present paper presents an effort to predict the urban heat island intensity in Athens based on limited available data series using various neural networks architectures. The overall effort is structured in three more sections. Section 2 provides the description of the region and the experimental sites. Section 3 analyses the selection and configuration of ANN while Section 4 includes the experimental results and discussion. Finally, Section 5 summarises the conclusions.

## 2. Experimental site description

The Greater Athens Area (GAA) is situated on a small peninsula located on the southeastern edge of the Greek mainland (Fig. 1). It is divided by high mountains in three main parts, which are connected by small openings. The central part is the Athens basin which covers an area of 450 km$^2$, with a population density of 8000 inhabitants per square kilometer, with the main axis orientated from SSW to NNE. Athens basin is surrounded by high mountains in the north (Parnitha, 1426 m), in the west (Egaleo, 458 m) and in the east (Hymettus, 1026 m and Penteli, 1107 m), while it is open to the sea from the south (Saronikos Gulf). The other parts of the Athens area are the Thriassion plain west of the Athens basin and the Mesogia plain in the east. There are only small openings through which the Athens basin communicates with these plains as well as the rest of Greek mainland. These openings play an important role in air mass exchange between the Athens basin and the Thriassion and Mesogia plains.

The city of Athens is characterised by a strong heat island effect, mainly caused by the accelerated industrialisation and urbanisation during recent years. From previous measurements' analysis is found that maximum heat island intensity in the Athens centre is almost 16 °C while the mean value for the major central area of Athens reaches 12 °C. Also, absolute maximum temperatures in the central area is close to 15 °C higher than in the suburban areas, while absolute minimum temperatures are up to 3 °C higher in the centre (Santamouris, 2001).

In a study performed by Livada et al. (2002) reporting the results of the heat island study in Athens, it is found that near the sea, the air temperatures are higher in the cold period due to the influence of the sea which supports the maintenance of high air temperatures. It is also reported that high air temperatures during the hot period of the year or low air temperatures in the cold period is mostly related to the synoptic weather conditions and it cannot reasonably considered as an index for the heat island effect development.

The increase of the cooling load in Athens and the ecological footprint of urban heat island is studied by Santamouris, Paraponiaris, et al. (2007) and Santamouris, Pavlou, et al. (2007). Given the actual penetration of air conditioning in the country, the ecological footprint due to the heat island ranges 1.5–2 times the city's surface area. Moreover the maximum potential ecological footprint provided that all buildings are air conditioned is almost


**Fig. 1.** The location of the 14 meteo station in the GAA.

**Table 1**
The location of the 14 experimental sites.

| *i* | Municipality | Latitude | Longitude |
|---|---|---|---|
| 1 | Egaleo | 37°59′50″ | 23°40′5″ |
| 2 | Korydalos | 37°58′45″ | 23°38′33″ |
| 3 | Haidari | 38°0′45″ | 23°39′35″ |
| 4 | Ag. Varbara | 37°59′22″ | 23°39′37″ |
| 5 | Peristeri | 38°0′47″ | 23°41′43″ |
| 6 | Kamatero | 38°3′35″ | 23°42′50″ |
| 7 | Zefyri | 38°4′7″ | 23°43′4″ |
| 8 | Ilioupoli | 37°55′58″ | 23°45′29″ |
| 9 | Petroupoli | 38°2′26″ | 23°41′16″ |
| 10 | Agii Anargyri | 38°1′34″ | 23°43′3″ |
| 11 | Xalandri | 38°0′44″ | 23°39′34″ |
| 12 | Ilion | 38°1′54″ | 23°42′27″ |
| 13 | Kaissariani | 37°58′8″ | 23°45′41″ |
| 14 | National Observatory of Athens (reference site) | 37°58′24″ | 23°43′5″ |

110,000 ha. The cost to compensate the heat island is calculated close to 4.13 M€/year or 164 € per household. The additional peak cooling electrical load to compensate the heat island is 82.4 MW.

In the present effort to predict the urban heat island effect in the area of Athens, a network of 14 meteorological stations has been set up corresponding to the 13 Athens municipalities plus the reference station (Table 1). The meteorological stations are placed on the administrative municipalities' buildings and are all 2 m above ground, north oriented, shaded and ventilated. Each meteorological station contains a fully calibrated high precision data logger (Tiny Tag data loggers) that measures air temperature every 15 min.

The sensors' characteristics are:

- Reading resolution 0.02 °C or better.
- Range −40 °C to +125 °C.
- Temperature stability ±0.01 °C/°C change from 25 °C.

In addition, other meteorological data (solar radiation, wind velocity, etc.) are collected from the National Observatory of Athens located at Thission, Athens (N′ 37° 58', E′ 23° 43'). The specific site is in a greenery area and is considered as the reference station of the overall analysis although it is positioned almost in the centre of the peninsula. The experimental period started on April 2009 in the framework of BRIDGE project (www.bridge-fp7.eu). The present analysis uses data for one-year period (from April 2009 until May 2010) targeting to minimise the need for long term historic data.

## 3. Application of ANN for urban heat island intensity prediction

### 3.1. Data sets

The measured and collected data are used as input in order to develop the ANN model and prediction procedure.

The input parameters for the neural network are as follows:

(i) Date to represent the yearly climatic variations (the date is converted into the number of days starting from the 1st of January) and ranges within [1,365].
(ii) Time, the time is converted into minutes of the day and ranges within [0,1380].
(iii) Ambient temperature (°C) measured by the various experimental sites described in the previous section.
(iv) Global solar radiation (W/m$^2$) measured by the National Observatory of Athens.

Neural networks generally provide improved performance when the data are normalised. The use of original data as input to the neural network may cause a convergence problem. All the temperature and global solar radiation data sets are, therefore, normalised in the range [−1,1] by dividing the difference between the actual value $x$ and minimum values by the difference between the maximum $x_{max}$ and minimum values $x_{min}$, i.e.

$$x_{nor} = \frac{x - x_{min}}{x_{max} - x_{min}}$$

The main goal of normalisation, in combination with the weight initialisation, is to allow the squashed activity function to work at least at the beginning of the learning phase. Thus, the gradient, which is a function of the derivative of the non-linearity, will always be different from zero. At the end of each algorithm, the outputs are transformed into its original data format.

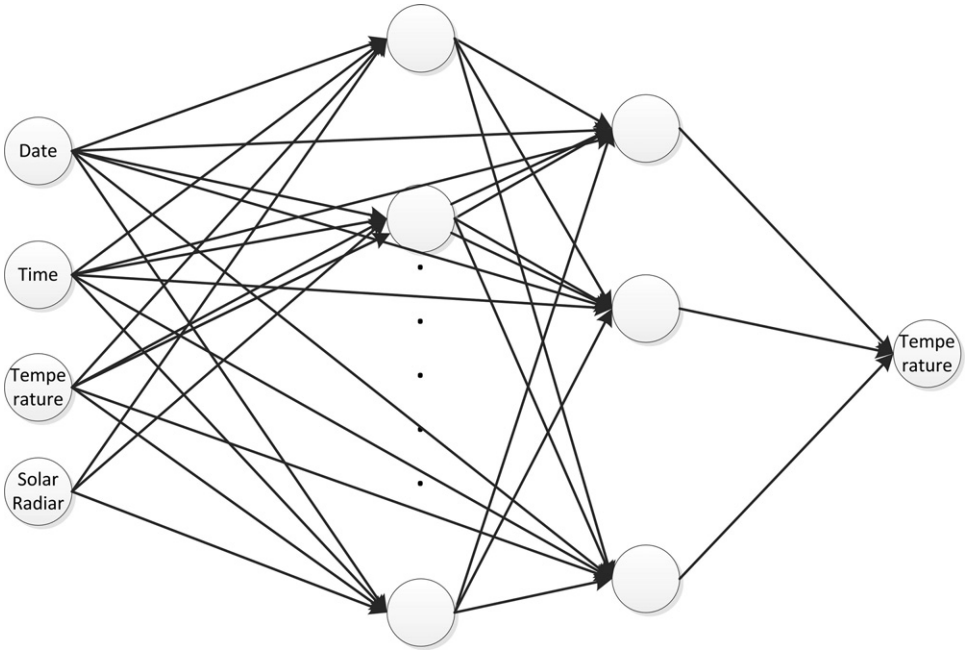


**Fig. 2.** Schematics diagram for the Cascade neural network.

### 3.2. The neural networks architecture

The prediction problem using neural network models can be separated into three steps or sub problems: designing the neural network architecture, conducting the learning or training process, and testing.

#### 3.2.1. The NN architecture design

In the present study three different neural networks are chosen:

(i) The Cascade NN (Fig. 2) which consists of the input layer, the layer of output neurons, and one or more hidden layers. The first layer has weights coming from the inputs and each subsequent layer has weights coming from the input and all previous layers. All layers have biases. The last layer is the network output (Hedayat, Davilu, Barfrosh, & Sepanloo, 2009).
(ii) The Elman NN (Fig. 3) which can be viewed as a Feed-Forward neural network with an additional set of inputs from the context layer (Song, 2010).
(iii) The Feed-Forward NN has all of the data information flows in one direction. The neurons of one layer are connected with the neurons of the following layer and there is no feedback (Fig. 4).

The selection of the networks' architecture is based on various results presented in the literature as well as in a preliminary trial and error procedure for various neural networks' types. Apart from the three above mentioned types, the NARX, Hopfield and Learning Vector Quantization (LVQ) neural networks are also tested without providing any encouraging results for the specific problem.

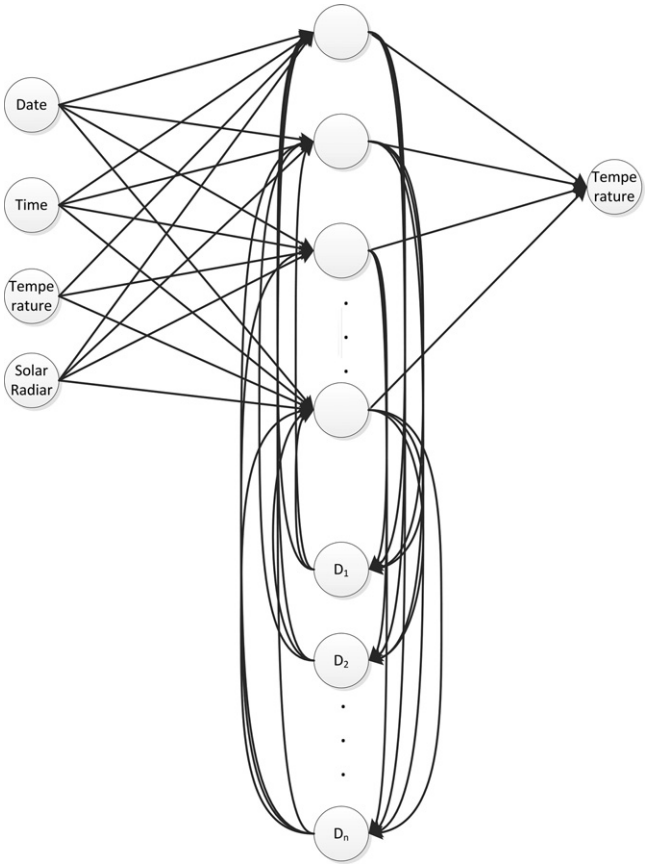


**Fig. 3.** Schematics diagram for the Elman neural network.

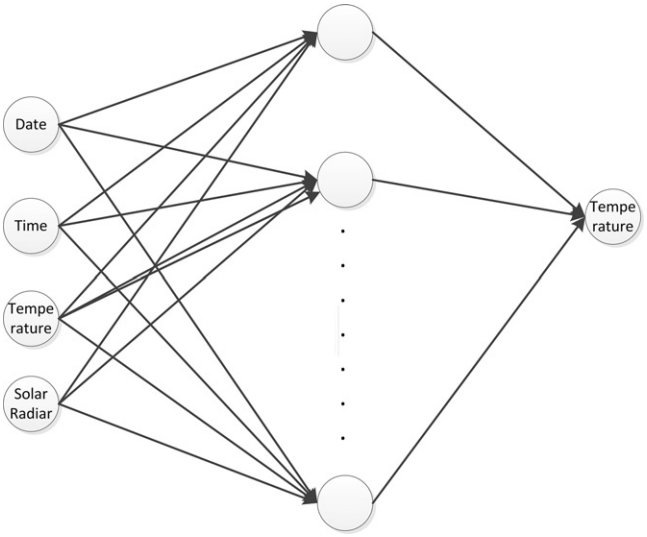


**Fig. 4.** Schematics diagram for the Feed-Forward neural network.

#### 3.2.2. The learning and training process

For each different neural network architecture the optimal training function, transfer or activation function, hidden layers and number of neurons are investigated. Each neural network consists of one to three hidden layers with 20–40 neurons each, followed by an output layer of one neuron. For all three neural networks (Cascade, Elman and Feed Forward) the following training functions are considered:

- Levenberg-Marquardt (trainlm).
- Scaled conjugate gradient (trainscg).
- BFGS quasi-Newton (trainbfg).
- Gradient descent (traingd).
- Gradient descent with momentum and adaptive learning rate (traingdm).
- Resilient back propagation training function (traingnrp).

The tangent sigmoid function is used as transfer function (Fig. 5) for all the NN.

Each neural network is trained using all the above training functions for the datasets from the Koridalos station for 1-h and 24-h prediction horizon respectively. The Koridalos site is randomly selected and the results are validated by the implementation of the same procedure in the Peristeri experimental site (see Tables 2 and 3).

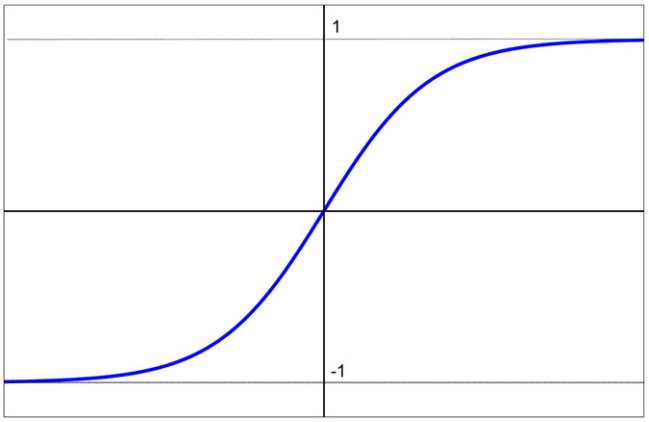


**Fig. 5.** Tangent sigmoid function.

**Table 2**
Performance comparison of difference training functions for Koridalos site.

| Training function | 1 h | | | 24 h | | |
|---|---|---|---|---|---|---|
| | Mean value | Standard deviation | MSE | Mean value | Standard deviation | MSE |
| Feed Forward | | | | | | |
| trainlm | 2.220 | 1.601 | 0.621 | 2.513 | 2.274 | 0.955 |
| **trainscg** | **2.041** | **1.385** | **0.484** | **2.291** | **1.970** | **0.820** |
| trainbfg | 22.355 | 12.376 | 38.023 | 30.355 | 17.376 | 45.023 |
| traingd | 7.471 | 7.215 | 6.859 | 8.873 | 6.997 | 8.285 |
| traingdm | 15.643 | 10.772 | 20.319 | 18.323 | 12.033 | 26.518 |
| traingnrp | 10.660 | 7.677 | 11.252 | 7.533 | 6.074 | 6.409 |
| Cascade | | | | | | |
| trainlm | 1.965 | 1.483 | 0.423 | 2.153 | 2.681 | 1.070 |
| trainscg | 1.954 | 1.342 | 0.393 | 2.163 | 1.978 | 0.773 |
| **trainbfg** | **1.666** | **1.084** | **0.593** | **0.942** | **0.845** | **0.131** |
| traingd | 3.606 | 3.259 | 1.812 | 3.476 | 3.140 | 1.668 |
| traingdm | 3.042 | 3.032 | 1.230 | 3.593 | 3.799 | 2.303 |
| traingnrp | 2.088 | 1.547 | 0.535 | 2.325 | 2.487 | 1.052 |
| Elamn | | | | | | |
| **trainlm** | **1.137** | **1.192** | **0.342** | **2.530** | **2.357** | **1.026** |
| trainscg | 1.897 | 1.295 | 0.367 | 1.517 | 1.085 | 0.303 |
| trainbfg | 1.975 | 1.321 | 0.614 | 1.254 | 0.967 | 0.652 |
| traingd | 2.560 | 1.723 | 0.780 | 1.556 | 1.294 | 0.314 |
| traingdm | 2.443 | 1.445 | 0.574 | 1.383 | 1.068 | 0.235 |
| traingnrp | 3.215 | 1.687 | 0.691 | 1.469 | 1.325 | 0.325 |

The best prediction performance is achieved by (see Tables 2 and 3):

- The Cascade neural network using the BFGS quasi-Newton as training function.
- The Elman neural network with the Levenberg-Marquardt as training function.
- Feed-Forward neural network with scaled conjugate gradient as training function.

### 3.2.3. *The testing process*

In this step the results from the three neural networks, for the various data sets are compared in order to examine the prediction accuracy. We choose the optimum results for each neural network. Figs. 6 and 7 present the measured versus the predicted values for Koridalos site for 1-h and 24-h prediction horizon respectively. The best fit of the measured to the observed data is achieved by the Elman followed by the Cascade and the Feed-Forward architecture.

The percentage error and the mean square error are utilised to calculate the difference between the measured and the predicted temperature values.

$$\text{Precent Error} = \frac{\text{Experiment} - \text{Theoretical value}}{\text{Theoretical value}} \times 100\%$$

The mean value (MV) and the standard deviation (SD) of the percentage error for each neural network architecture and for 1-h prediction horizon are $1.8 \pm 1.0\%$ for Elman, $2.8 \pm 2.2\%$ for Feed Forward and $2.4 \pm 1.5\%$ for Cascade. The same results apply for the 24-h prediction horizon as tabulated in Table 2. The mean squared error (MSE) of the three neural networks and for Koridalos site is for Feed-Forward 1.12, for Cascade 0.65 and for Elman 0.35.

The above results show that the most suitable NN architecture for the urban heat island intensity prediction is the Elman type using Levenberg-Marquardt as transfer function. The above results are verified by following the same procedure for another site, placed in a quite different location, i.e. the Peristeri site. The results of the analysis performed in Peristeri site are tabulated in

**Table 3**
Performance comparison of difference training function for Peristeri site.

| Training function | 1 h | | | 24 h | | |
|---|---|---|---|---|---|---|
| | Mean value | Standard deviation | MSE | Mean value | Standard deviation | MSE |
| Feed Forward | | | | | | |
| trainlm | 3.606 | 3.259 | 1.812 | 4.128 | 5.655 | 4.348 |
| **trainscg** | **3.174** | **2.457** | **1.407** | **3.087** | **3.087** | **2.253** |
| trainbfg | 7.707 | 5.638 | 9.454 | 14.607 | 10.348 | 23.870 |
| traingd | 9.201 | 7.230 | 12.596 | 7.677 | 5.402 | 6.144 |
| traingdm | 6.980 | 6.779 | 8.493 | 10.595 | 8.019 | 13.464 |
| traingnrp | 6.890 | 6.391 | 7.157 | 11.877 | 10.265 | 14.669 |
| Cascade | | | | | | |
| trainlm | 2.930 | 2.269 | 1.166 | 3.691 | 3.908 | 2.745 |
| trainscg | 2.805 | 2.155 | 1.043 | 2.764 | 2.682 | 1.454 |
| **trainbfg** | **2.890** | **2.281** | **1.157** | **2.912** | **2.636** | **1.411** |
| traingd | 6.317 | 7.253 | 6.964 | 5.172 | 5.109 | 3.599 |
| traingdm | 6.831 | 5.684 | 5.880 | 4.689 | 4.776 | 3.540 |
| traingnrp | 2.994 | 2.282 | 1.233 | 3.381 | 4.217 | 2.475 |
| Elamn | | | | | | |
| **trainlm** | **2.234** | **1.351** | **0.911** | **1.142** | **0.736** | **0.151** |
| trainscg | 3.299 | 2.041 | 1.160 | 1.268 | 0.923 | 0.173 |
| trainbfg | 3.754 | 2.545 | 2.840 | 3.412 | 1.785 | 0.985 |
| traingd | 2.886 | 1.920 | 0.520 | 1.835 | 1.575 | 0.571 |
| traingdm | 3.315 | 5.818 | 3.122 | 3.202 | 7.685 | 3.652 |
| traingnrp | 3.125 | 2.958 | 2.958 | 3.587 | 2.218 | 2.504 |

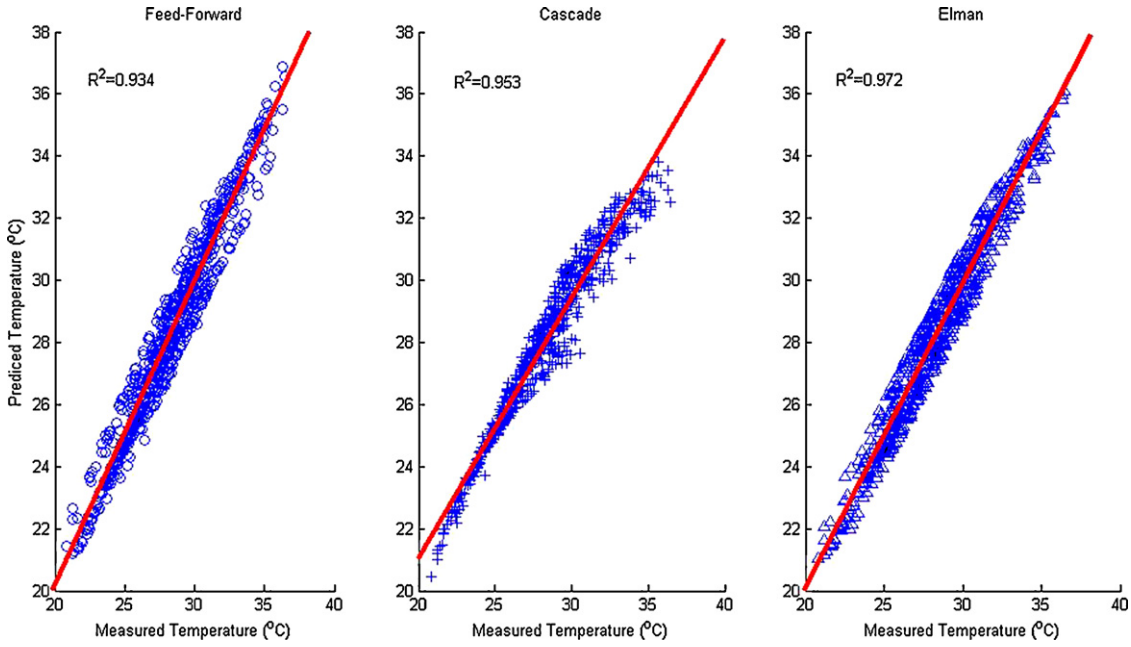


**Fig. 6.** Comparison between the three different ANN for 1-h prediction horizon.

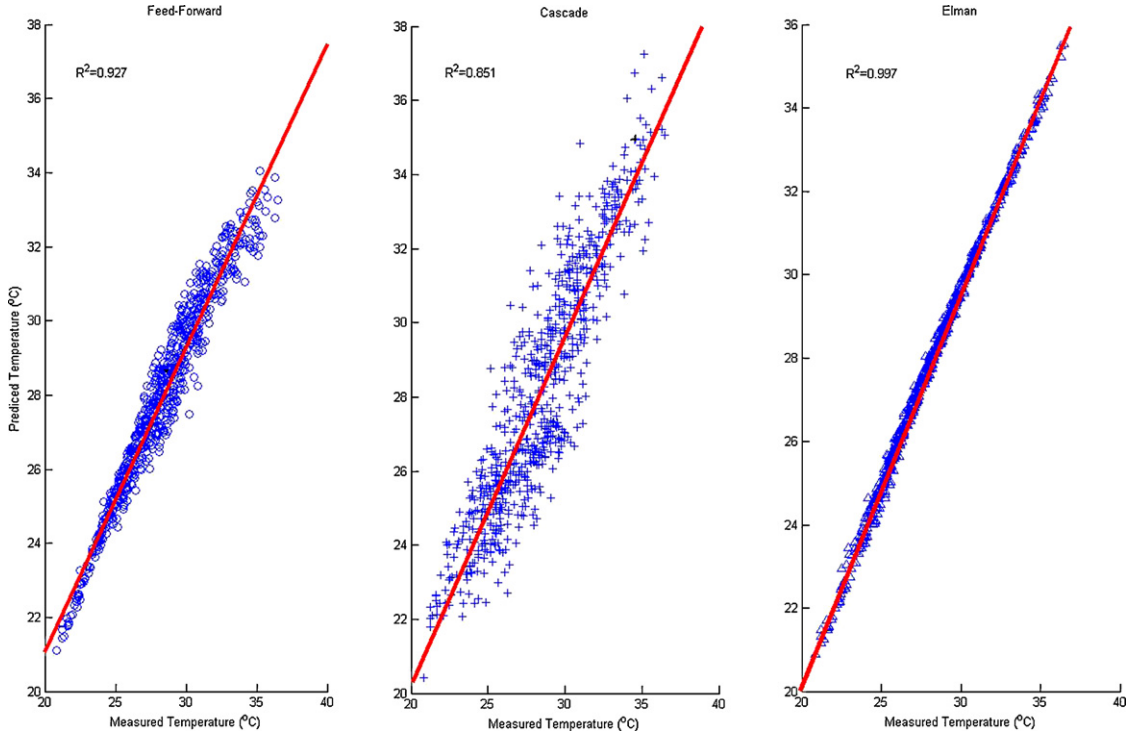


**Fig. 7.** Comparison between different ANN for 24-h prediction horizon.

Table 3 and verify that the optimum neural network is the Elman. The specific network architecture is then used for predicting the urban heat island intensity in all sites.

## 4. Results and discussion

Training and verification of the ANN is performed using the data collected during the period from 06/04/2009 to 07/09/2009 for each experimental site. Therefore the training and verification period is shortened to five months.

The data are fed into the ANN as blocks of 24 values corresponding to each hour of the day. The neural network has a training period of 40–60 days. The remaining data are used to verify the quality of network and adaptation of the neural network to the new data.

Figs. 8 and 9 show the measured and predicted temperatures of 5 different locations (i.e. Ilion, Zefyri, Petoupoli, Aegaleo and Agii Anargyri) and for two different dates 19–20/06/2009 and 05–06/07/2009 respectively. As we can see in Fig. 8, the diurnal fluctuation of temperatures is very smooth and is followed by the 1-h and 24-h Elman prediction algorithms quite accurately. Furthermore, although the daily temperature fluctuations depicted in

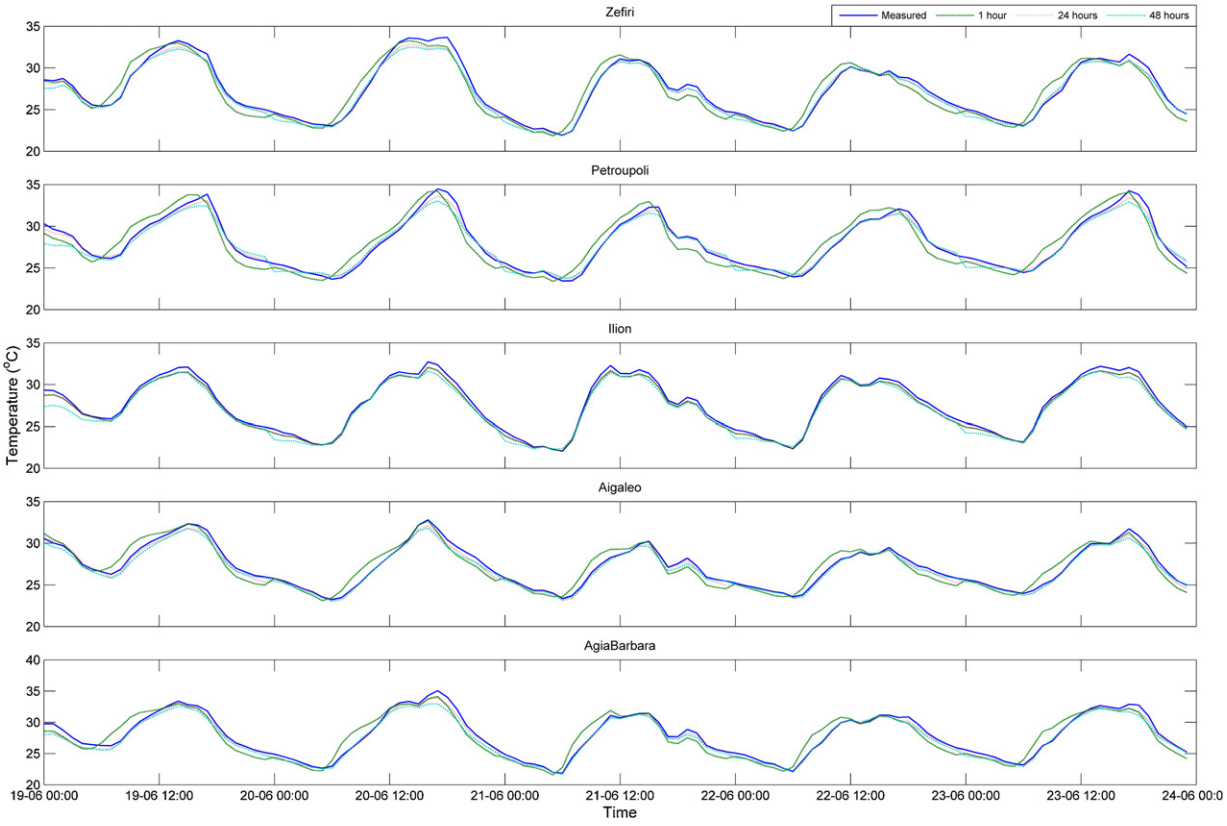


**Fig. 8.** Measured–predicted temperatures for 19–20/06/2009.

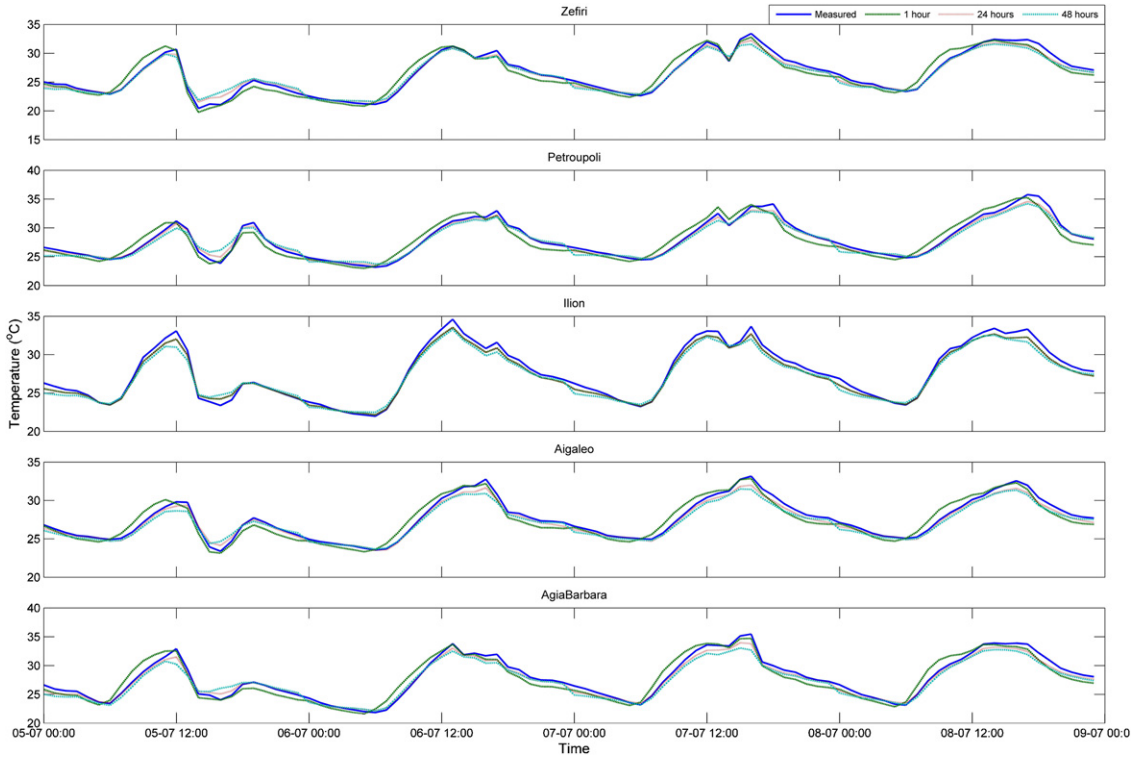


**Fig. 9.** Measured–predicted temperatures for 05–06/07/2009.

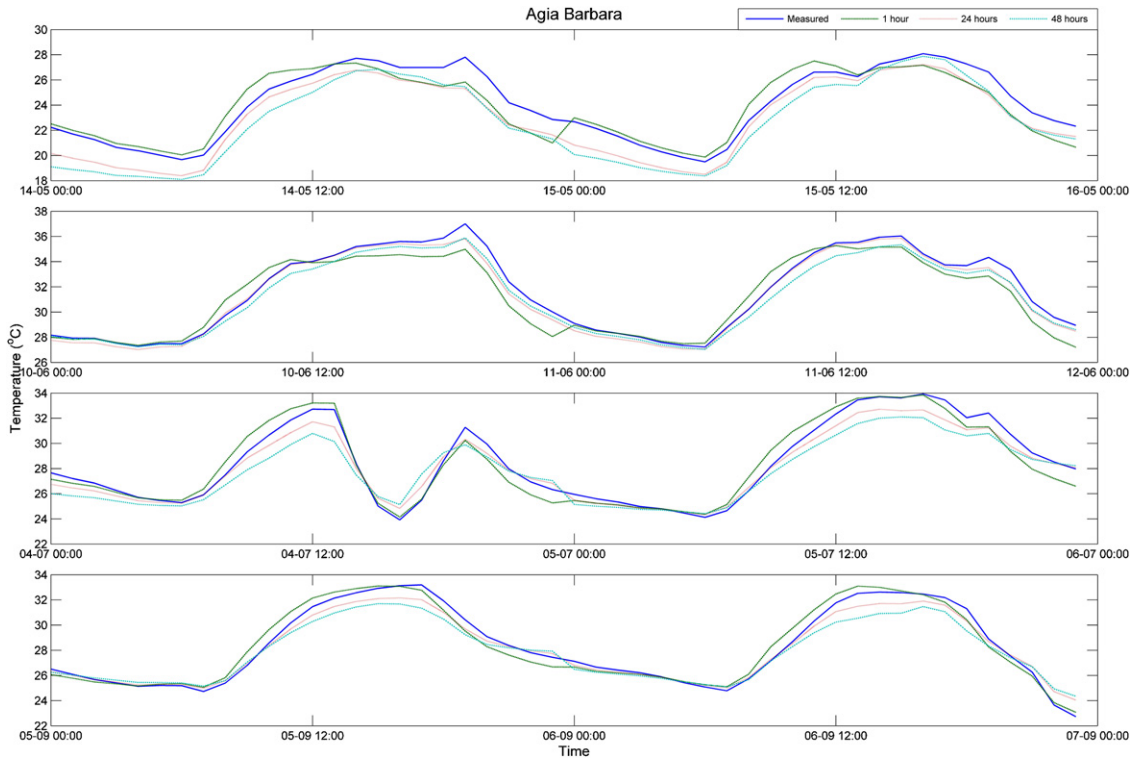


**Fig. 10.** Monthly comparison for measured–predicted temperatures of Haidati meteo station.

Fig. 9 are not as smooth and predictable, the Elman NN manages to follow the measured data most of the time.

Another significant aspect of the proposed neural network architecture that should be examined is the alterations in prediction accuracy due to seasonal variations and the necessity to retrain the network when the season changes. In Figs. 10 and 11 the measured and predicted temperatures are depicted for Haidari and Agia Barbara experimental sites. Although the prediction accuracy is not always the highest possible, especially for the 48-h prediction horizon, the overall prediction accuracy does not change significantly

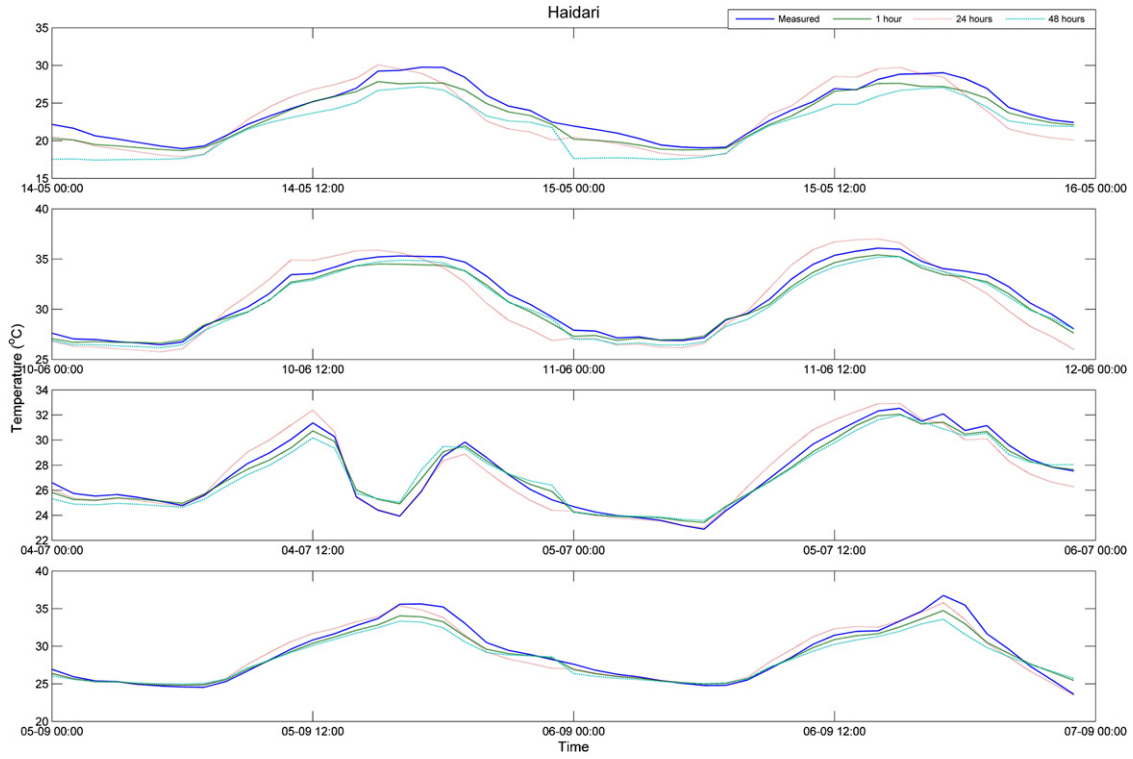


**Fig. 11.** Monthly comparison for measured–predicted temperatures of Agia Barbara meteo station.

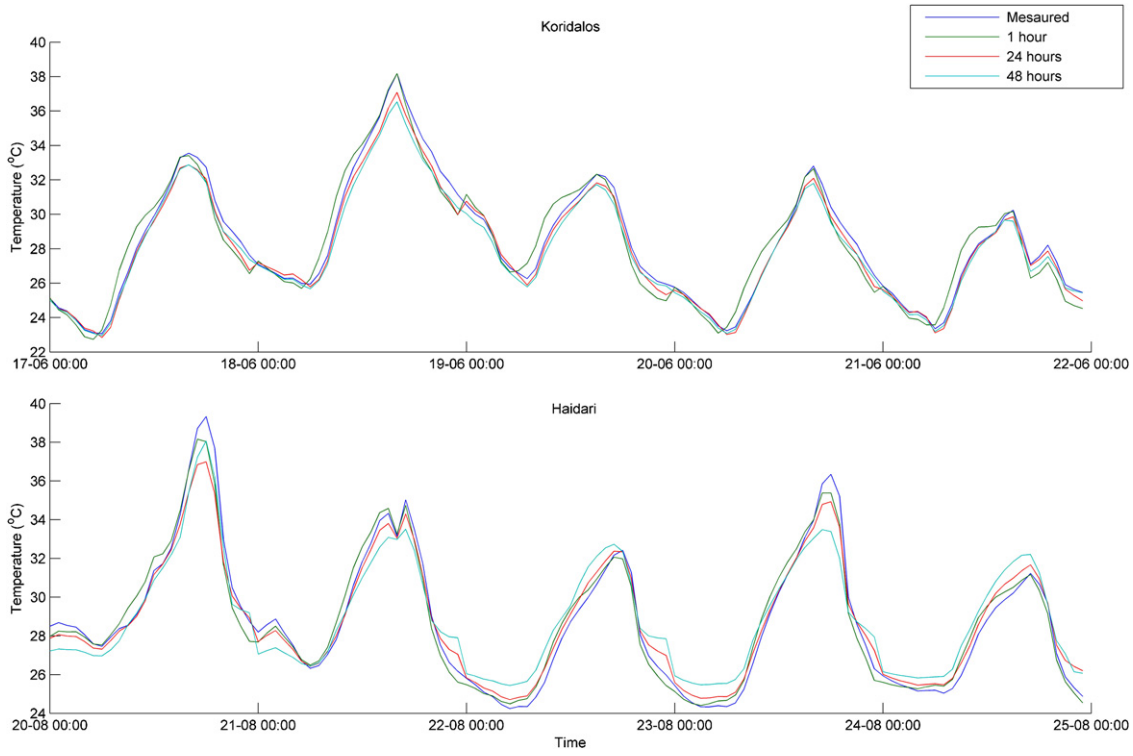


**Fig. 12.** Response of the ANN to weather changes.

with the seasonal changes. The seasonal changes of the standard deviation between the measured and predicted values for Haidari and Agia Barbara sites are tabulated in Table 4. Another significant aspect is the methodology's response to different weather conditions or during weather changes. For this reason the ANN's response is studied for two experimental sites, i.e. Koridalos and Haidari as well as for day to day temperature changes (Fig. 12). As we can see in the specific figure, although outdoor temperature is consid-

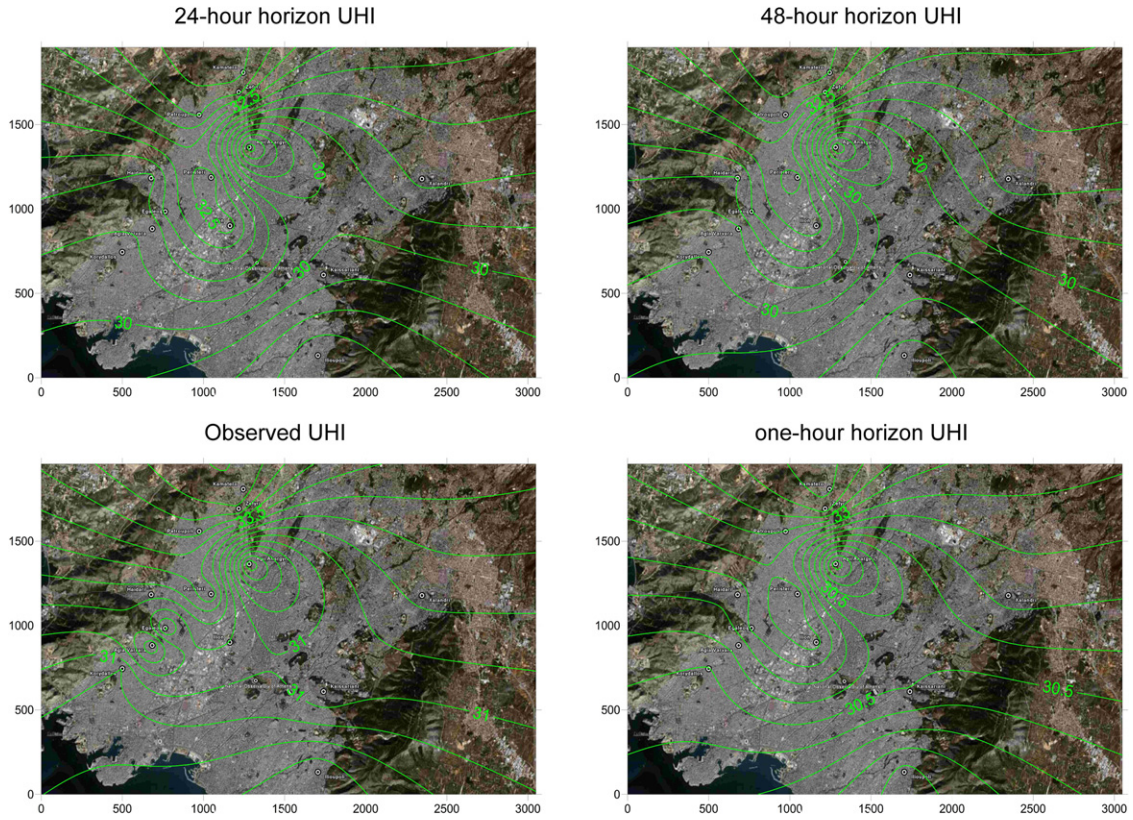


**Fig. 13.** The UHI in Athens during 01/07/2009.

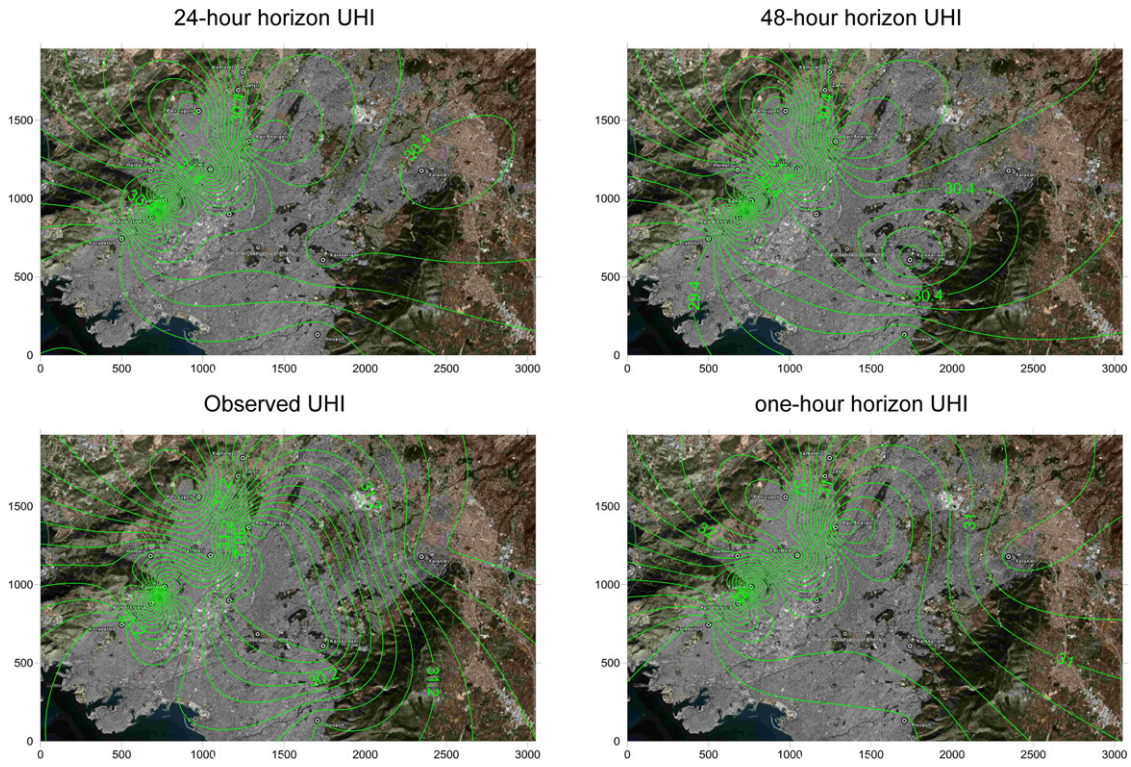


**Fig. 14.** The UHI in Athens during 18/06/2009.

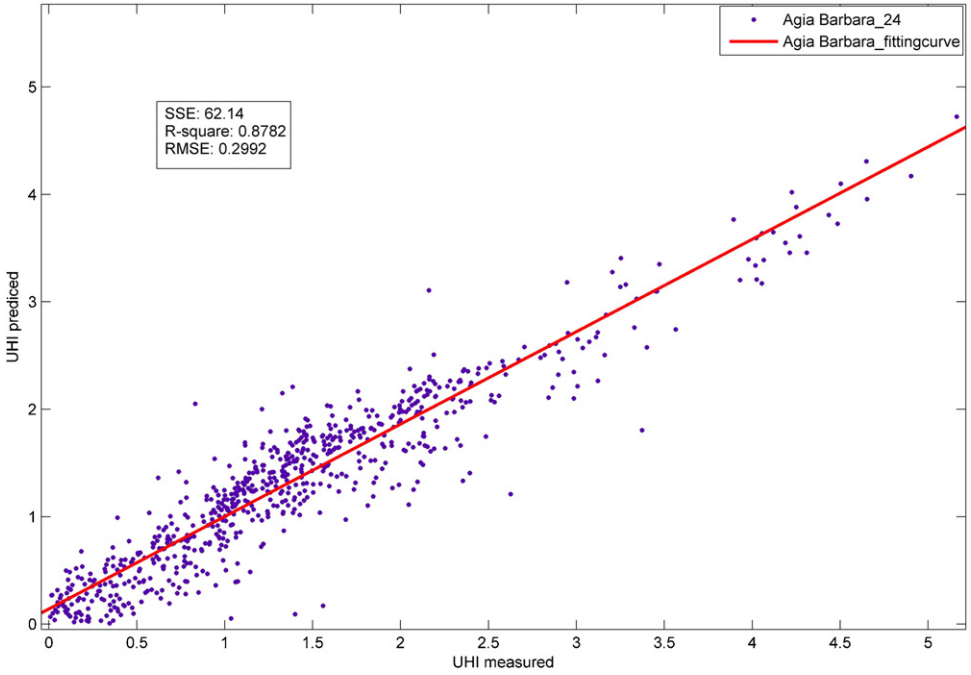


**Fig. 15.** The UHI measured versus UHI 24 h predicted for the Agia Barbara site.

**Table 4**
Seasonal variations of standard deviation between measured and predicted temperatures for Agia Barbara and Haidari sites.

| Prediction horizon | Agia Barbara | | | Haidari | | |
|---|---|---|---|---|---|---|
| | 1 h | 24 h | 48 h | 1 | 24 | 48 |
| 12/5/2009–31/6/2009 | 0.5516 | 0.9301 | 0.7581 | 0.5532 | 1.4003 | 1.0013 |
| 1/6/2009–30/6/2009 | 0.4392 | 0.8087 | 0.733 | 1.0013 | 1.0267 | 0.5104 |
| 1/7/2009–31/7/2009 | 0.7787 | 0.793 | 1.2449 | 0.5767 | 0.8057 | 0.9998 |
| 1/8/2009–31/8/2009 | 0.4127 | 0.5587 | 0.9892 | 0.5326 | 0.5731 | 1.0996 |
| 1/9/2009–6/9/2009 | 0.4682 | 0.5061 | 0.93 | 0.7029 | 0.7274 | 1.1727 |

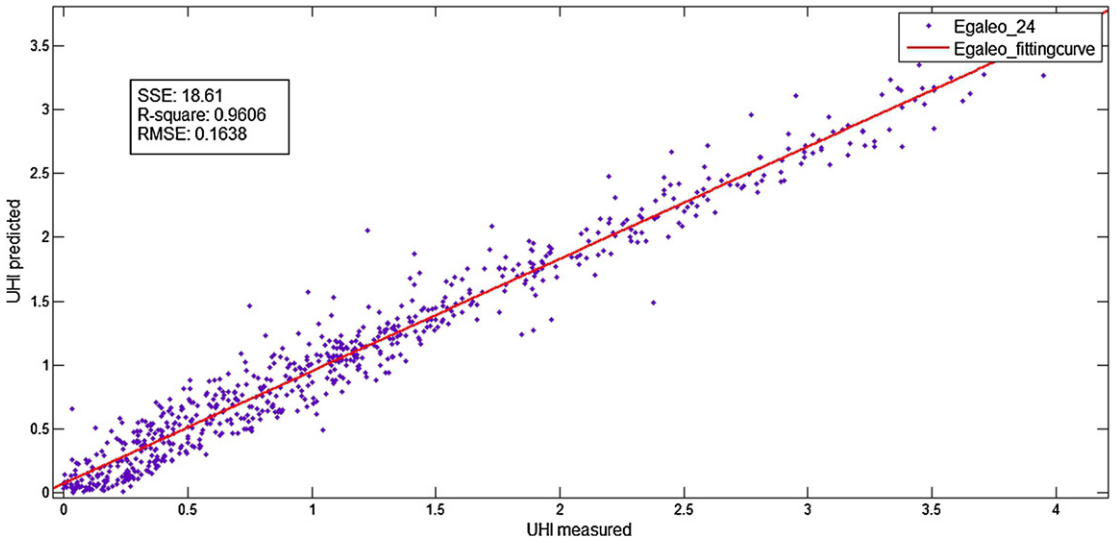


**Fig. 16.** The UHI measured versus UHI 24 h predicted for the Egaleo site.

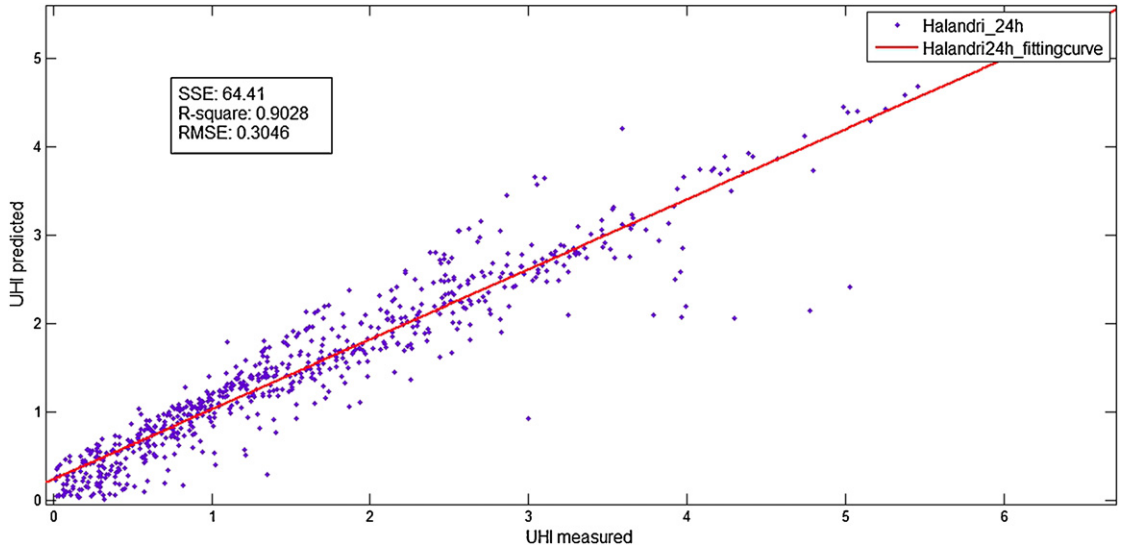


**Fig. 17.** The UHI measured versus UHI 24 h predicted for the Halandri site.

erably decreased from 19/6/2009 to 20/6/2009, and also increased from 23/8/2009 to 24/8/2009, the ANN follows this change in a successful manner especially for the 24-h prediction horizon.

Moreover isothermal images are developed to imprint the UHI intensity over Athens. The mapping of the region is performed is using Google Earth while the isothermal lines are added by Surfer 8 software. For each day that the UHI over Athens is analyzed, a set of four images is constructed to visualize the ANN prediction:

- The first image maps the isotherms over Athens using the measured data of the specific day and time.
- The second image represents the isotherms of Athens urban heat island based on the 1-h prediction results for the specific day and time.
- The third image maps the isotherms of Athens urban heat island based on the 24-h prediction results for the specific day and time.
- The fourth image plots the isotherms of Athens urban heat island based on the 48-h prediction results for the specific day and time.

Indicatively the isothermal maps of the UHI intensity over Athens for two days (i.e. 1/7/2009 and 18/6/2009) are illustrated in Figs. 13 and 14. The prediction of the maximum temperatures for the 1/7/2009 has a maximum error of 1.6 °C and 1.9 °C for the 24-h and 48-h prediction horizon respectively. Moreover the visualization of UHI intensity prediction shows that the isotherms of the 24-h prediction are very close to the actual measured ones while the 48-h prediction has a slightly different picture. Therefore the specific NN architecture and methodology followed is quite accurate for the 24-h prediction horizon.

The urban heat island intensity is then calculated versus the reference station, i.e. National Observatory of Athens. The predicted versus the measured urban heat island intensity for three sites (i.e. Agia Barbara, Egaleo and Halandri) and for 24-h prediction are depicted in Figs. 15–17 respectively. The figures show a satisfactory fitting with a RMSE less than 0.3 and $R^2$ to be close or higher than 0.9 for all three sites which represents a good prediction of the urban heat island intensity.

## 5. Conclusion and future prospects

Important heat island studies have been performed in Europe during the last decades showing that the deep understanding of the

phenomenon plays an important role in fighting its consequences to the climate change. Advanced artificial intelligence techniques such as neural networks offer on the other hand a valuable tool to be used for the prediction of the specific phenomenon. The neural networks prediction accuracy is mainly based on the quality and quantity of the available data.

The aim of the present paper was to investigate the feasibility of predicting the urban heat island phenomenon using a limited data series. The Athens case study was used to demonstrate the feasibility and accuracy of the overall approach.

The methodology presented in the present paper showed that the urban heat island intensity can be predicted quite accurately for at least a 24-h prediction horizon using a limited set of data.

Therefore the NN prediction methodology can be an important tool for peak energy load predictions during heat waves and hot summer days contributing to the demand and supply energy management.

## Acknowledgement

The research leading to these results has received funding from the European Community's Seventh Framework Programme (FP7/2007-2013) under grant agreement n° 211345 (BRIDGE Project).

## References

Akbari, H., Konopacki, S., & Pomerantz, M. (1999). Cooling energy savings potential of reflective roofs for residential and commercial buildings in the United States. *Energy*, *24*, 391–407.

Cartalis, C., Synodinou, A., Proedrou, M., Tsangrassoulis, A., & Santamouris, M. (2001). Modifications in Energy Demand in urban areas as a result of climate changes: An assessment for the southeast Mediterranean region. *Energy Conversion and Management*, *42*(14), 1647–1656.

Crutzen, P. (2004). New directions: The growing urban heat and pollution 'island' effect—Impact on chemistry and climate. *Atmospheric Environment*, *38*, 3539–3540.

Geros, V., Santamouris, M., Karatasou, S., Tsangrassoulis, A., & Papanikolaou, N. (2005). On the cooling potential of night ventilation techniques in the urban environment. *Energy and Buildings*, *37*(3), 243–257.

Hassid, S., Santamouris, M., Papanikolaou, N., Linardi, A., Klitsikas, N., Georgakis, C., et al. (2000). The effect of the Athens heat island on air conditioning load. *Energy and Buildings*, *32*, 131–141.

Hedayat, A., Davilu, H., Barfrosh, A. A., & Sepanloo, K. (2009). Estimation of research reactor core parameters using cascade feed forward artificial neural networks. *Progress in Nuclear Energy*, *51*(6), 709–718.

Jiang, D., Zhang, Y., Hu, X., Zeng, Y., Tan, J., & Shao, D. (2004). Progress in developing an ANN model for air pollution index forecast. *Atmospheric Environment*, *38*(40 SPEC.ISS.), 7055–7064.

Kolokotroni, M., Davies, M., Croxford, B., Bhuiyan, S., & Mavrogianni, A. (2010). A validated methodology for the prediction of heating and cooling energy demand for buildings within the urban heat island: Case-study of London. *Solar Energy*, *84*(12), 2246–2255.

Kolokotroni, M., Giannitsaris, I., & Watkins, R. (2006). The effect of the London urban heat island on building summer cooling demand and night ventilation strategies. *Solar Energy*, *80*(4), 383e92.

Livada, I., Santamouris, M., & Assimakopoulos, M. N. (2007). On the variability of summer air temperature during the last 28 years in Athens. *Journal of Geophysical Research*, *112*, D12103.

Livada, I., Santamouris, M., Niachou, K., Papanikolaou, N., & Mihalakakou, G. (2002). Determination of places in the great Athens area where the heat island effect is observed. *Theoretical and Applied Climatology*, *71*(3–4), 219–230.

Maqsood, I., Khan, M. R., & Abraham, A. (2004). An ensemble of neural networks for weather forecasting. *Neural Computer Applications*, *13*, 112–122.

Mihalakakou, M., Santamouris, N., & Papanikolaou, C. (2004). Cartalis simulation of the urban heat island phenomenon in Mediterranean climates. *Pure and Applied Geophysics*, *161*, 429–451.

Mihalakakou, P., Flokas, H., Santamouris, M., & Helmis, C. (2000). Application of neural networks to the simulation of the heat island over Athens Greece using synoptic types as a predictor. *Journal of Applied Meteorology*, *41*, 519–527.

Mirzaei, P. A., & Haghighat, F. (2010). Approaches to study urban heat island—Abilities and limitations. *Building and Environment*, *45*(10), 2192–2201.

Ruano, A. E., Crispim, E. M., Conceicão, E. Z. E., & Lúcio, M. M. J. R. (2006). Prediction of building's temperature using neural networks models. *Energy and Buildings*, *38*, 682–694.

Santamouris, M., Mihalakakou, G., Papanikolaou, N., & Assimakopoulos, D. N. (1999). A neural network approach for modelling the heat island phenomenon in urban areas during the summer period. *Geophysics Research Letters*, *26*(3), 337–340.

Santamouris, M. (2001). *Energy and Climate in the Urban Built Environment*. London: James and James Science Publishers.

Santamouris, M. (2007). Heat island research in Europe: The state of the art. *Advances in Building Energy Research*, *1*, 123–150.

Santamouris, M., Paraponiaris, K., & Mihalakakou, G. (2007). Estimating the ecological footprint of the heat island effect over Athens, Greece. *Climate Change*, *80*, 265–276.

Santamouris, M., Pavlou, K., Synnefa, A., Niachou, K., & Kolokotsa, D. (2007). Recent progress on passive cooling techniques advanced technological developments to improve survivability levels in low-income households. *Energy and Buildings*, *39*, 859–866.

Song, Q. (2010). On the weight convergence of Elman networks. *IEEE Transactions on Neural Networks*, *21*(3), 463–480.

Taha, H. (1994). Meteorological and photochemical simulations of the South Coast Air Basin. In H. Taha (Ed.), *Analysis of energy efficiency of air quality in the south coast air basin—Phase II, LBL-35728* (pp. 161–218). Lawrence Berkeley Laboratory.

Tasadduq, I., Rehman, S., & Bubshait, K. (2002). Application of neural networks for the prediction of hourly mean surface temperatures in Saudi Arabia. *Renewable Energy*, *36*, 545–554.

Yi, J., & Prybutok, V. R. (1996). A neural network model forecasting for prediction of daily maximum ozone concentration in an industrialized urban area. *Environmental Pollution*, *92*(3), 349–357.